



**HAL**  
open science

# Discrete element modeling of interface debonding behavior in composite material: Application to a fragmentation test

B. D. Le, F. Dau, D. H. Pham, T. D. Tran

► **To cite this version:**

B. D. Le, F. Dau, D. H. Pham, T. D. Tran. Discrete element modeling of interface debonding behavior in composite material: Application to a fragmentation test. *Composite Structures*, 2021, 272, pp.114170. 10.1016/j.compstruct.2021.114170 . hal-03482883

**HAL Id: hal-03482883**

**<https://hal.science/hal-03482883>**

Submitted on 2 Aug 2023

**HAL** is a multi-disciplinary open access archive for the deposit and dissemination of scientific research documents, whether they are published or not. The documents may come from teaching and research institutions in France or abroad, or from public or private research centers.

L'archive ouverte pluridisciplinaire **HAL**, est destinée au dépôt et à la diffusion de documents scientifiques de niveau recherche, publiés ou non, émanant des établissements d'enseignement et de recherche français ou étrangers, des laboratoires publics ou privés.



Distributed under a Creative Commons Attribution - NonCommercial 4.0 International License

# Discrete element modeling of interface debonding behavior in composite material: Application to a fragmentation test

B.D LE<sup>a</sup>, F. Dau<sup>b,\*</sup>, D.H. Pham<sup>a</sup> and T.D. Tran<sup>a</sup>

<sup>a</sup>National University of Civil Engineering, Hanoi, Vietnam

<sup>b</sup>Department of Durability of Materials, Assemblies and Structures (DuMAS), Arts et Metiers ParisTech, I2M, UMR 5295 CNRS F-33400, Talence, France

## ARTICLE INFO

### Keywords:

Composite material  
Interface debonding  
Discrete Element Model  
Cohesive law  
Bi-disperse medium

## ABSTRACT

This paper presents a 3D simulation of interface debonding in composite material using 3D Discrete Element Model (DEM). The simulation is based on the experimental results obtained by Guillebaud-Bonnafous and al. [19]. A single fragmentation testing of a singer impregnated hemp yarn embedded into a epoxy matrix was investigated. In DEM, matrix and yarn are supposed to be brittle materials and follow a linear fracture model. The discrete elements of matrix are connected by the cohesive beams whereas the one of yarn are connected by the spring links. The cohesive contact laws are implemented to model interface debonding between yarn and matrix (yarn/matrix). Piecewise linear elastic laws usually used in Cohesive Zone Models are retained in this work. The numerical results obtained by DEM are compared with experiment data and finite element modeling on the stress-strain curve and the fragmentation process in yarn during the test. This comparison allows to validate the models used in DEM. To reduce the discrete elements number and save computational time, the bi-disperse medium in DEM for matrix and yarn is specifically elaborated in this study.

## 1. Introduction

In composite material, the interface is commonly the surface formed by a common boundary between fiber and matrix. It plays an important role to transfer the load from the reinforcement matrix to fiber. The failure mode, the fracture toughness of composite material are directly influenced by the interface properties [25]. When loading a composite, the damage and fracture mechanisms can occur in the matrix and/or in the fiber and/or at fiber/matrix interface. Interfacial debonding may be a significant mechanism of energy absorption leading to the failure of a composite.

To characterize the interface debonding properties, several experimental technics have been used, such as the single fiber pull-out test [8, 35, 40], the push-out test [7, 57], the microbond test [36, 41] and the fragmentation test [4, 51]. In previous tests, the fiber/matrix interface is supposed to be under pure shear behavior. The mechanical properties (shear strength, friction,...) are identified from the experimental results.

Thanks to the simplicity in specimen preparation, convenient testing and more informations about damage processes can be obtained, the fragmentation test is widely used [15, 11]. This test is realized by applying a tensile load to a single fiber embedded in a matrix (Fig.1a). The tensile stress in the matrix transfers to the fiber via fiber/matrix interface. When the tensile load increases, the first crack appears in the fiber, because the failure strain of the fiber is much lower

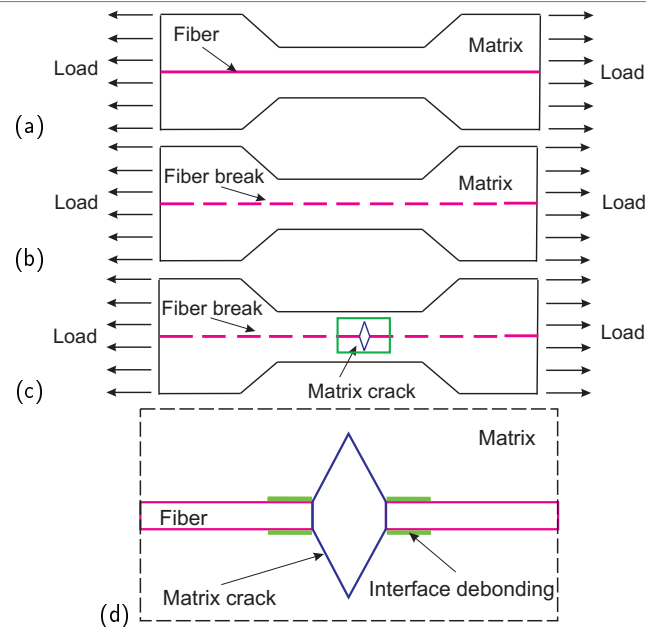


**Figure 1:** The fragmentation test: (a) typical specimen; (b) saturation of fragmentation process, (c) matrix crack and (d) matrix crack and interface debonding

than that of matrix. Then the fiber continues to break into smaller fragments. This state is defined as the saturation of fragmentation process in the fiber (Fig.1b). During the test, the tensile stress in fiber, matrix and fiber/matrix interface redistribute around the fiber break. The damage in the specimen depends on the fiber/matrix interface strength. For a high fiber/matrix interface strength, the crack occurs and propagates into the fiber and the matrix (Fig.1c). Contrariwise, the interface debonding occurs between fiber and matrix (Fig.1d).

\* This document is the results of the research project funded by The National Foundation for Science and Technology Development (NAFOS-TED) of Vietnam for project "Modeling of delamination, crack initiation and propagation in composite material using 3D Discrete Element Method"; Code 107.02-2017.13.

\*Corresponding author

frederic.dau@ensam.eu (F. Dau)

ORCID(s):

To study the fiber/matrix interface behavior, various numerical models have been used. Ramzan Babaei and al. [6] have developed a new interface model based on continuum damage mechanics (CDM) to investigate the fiber-matrix interfacial debonding in the composite material in 2D. Kelly and Tyson [23] propose a constant shear stress model to study the interface properties. This model allows to estimate the interfacial shear strength from the final distribution of fiber fragmented lengths. However, the constant shear stress model is inconsistent while considering matrix plasticity [41, 44]. The fracture mechanics models is used in other studies [24, 31] to identify the interfacial fracture toughness, based on debonding growth. The limitation is then to estimate the microscopic damage process (e.g. fiber/matrix interface debonding, matrix crack). In order to improve the limits of these models, the Cohesive Zone Model (CZM) is proposed [9, 12, 45]. It allows to clarify the physical and mechanical behavior of the interface debonding, the fragmentation process.

In some studies, the CZM have been implemented into continuum method, like Finite Element Method (FEM) and Extended Finite Element Method (XFEM) [20, 5, 34, 43, 38]. The tensile stresses transfer from matrix to fiber during the fragmentation test. The effects of micro damage modes (matrix crack, interface debonding) on fragmentation have been studied [18, 50, 39, 22, 17]. However, arranging cohesive element everywhere in a model to predict complex cracking paths is not the suitable way to do.

In order to overcome these difficulties of continuum model, the DEM is a relevant alternative. DEM is capable to naturally capture the damages and their growth in composite medium without preset paths [32]. It is not necessary to remesh during the crack propagation. Several studies using DEM to model the fracture behavior of composite materials in 2D are presented in [55, 56, 37, 53, 52]. The purpose of this research is to use 3D Discrete Element Method for modeling the fracture behavior and fiber/matrix interface debonding of composite material. Matrix and fiber are supposed to be brittle materials and follow a linear fracture model. Cohesive Contact Model (CCM) are implemented in DEM to model interface debonding between fiber and matrix. The DEM simulation is based on the experimental results obtained by Guillebaud-Bonafous and al. [19].

In this paper, the DEM is first recalled. Then, the geometrical modelization of the composite medium as a bi-disperse medium is presented; a 0° oriented single yarn is considered at this stage. Next, the mechanical modelization for yarn, matrix and yarn/matrix interface with CCM is described. The following sections are devoted to numerical fragmentation tests and conclusions.

## 2. Discrete Element Model in GranOO workbench

The DEM was originally developed to model movements within granular materials [13]. More recently, this method was extended to model the fracture behavior of continuous materials, such as brittle materials [29, 30, 26], concrete and

rocks [46, 33, 48], and composite [28, 47, 55]. In these studies, the material is modeled by an agglomerate of Discrete Elements (DEs) interacting through bilateral cohesive links to ensure the behavior of a continuous material (Fig.2a). Spherical DEs (3D [13, 10], circular (2D) [49, 29], or polyhedral [27, 14] are commonly used in DEM. On the other hand in accordance with the physical properties of material, springs and dampers links (Fig.2b), or cohesive beams (Fig.2c) are usually employed. The microscopic parameters of cohesive links are identified by a calibration process. Then, elasticity, plasticity, viscosity and more complex behavior of material can be addressed through these links. To model a continuum material by DEM, the following four steps are required: (1) Building of the discrete domain, (2) Choice of the rheological model of the bonds, (3) Quantification of the rheological model and (4) Implementation and application.

The discrete element software GranOO (Granular Object Oriented workbench) developed in the lab [1] is used in this study. The numerical resolution is based on Verlet velocities explicit dynamics integration scheme [16]. This scheme allows to calculate the discrete element position and velocity (linear and angular) at each time step (from Eq.1 to Eq.4):

$$\vec{p}(t + dt) = \vec{p}(t) + dt\vec{p}(t) + \frac{dt^2}{2}\vec{p}(t) \quad (1)$$

$$\vec{p}(t + dt) = \vec{p}(t) + \beta_1 \frac{dt}{2}(\vec{p}(t) + \vec{p}(t + dt)) \quad (2)$$

$$\vec{q}(t + dt) = \vec{q}(t) + dt\vec{q}(t) + \frac{dt^2}{2}\vec{q}(t) \quad (3)$$

$$\vec{q}(t + dt) = \vec{q}(t) + \beta_2 \frac{dt}{2}(\vec{q}(t) + \vec{q}(t + dt)) \quad (4)$$

where:

- $t$  is the current time and  $dt$  is the integration time step.
- $\vec{p}(t)$ ,  $\vec{p}(t)$ ,  $\vec{p}(t)$  is the discrete element linear position, velocity and acceleration.
- $\vec{q}(t)$ ,  $\vec{q}(t)$ ,  $\vec{q}(t)$  is the discrete element angular position, velocity and acceleration.
- $\beta_1$ ,  $\beta_2$  is the numerical damping factor.

In present work, 3D spherical shape is used for discrete element. To obtain a mechanical behavior representative of continuous medium, a uniform dispersion of 25% between maximum and minimum spheres' radius is selected. Otherwise, the cohesive beams are implemented to connect the discrete elements (Fig.3a). Fig.3b shows the cohesive beam in a loaded state involving displacements between centers ( $O_1O_2$ ) and rotations ( $\theta_1\theta_2$ ) of the spherical discrete elements. These beams have a circular cylindrical shape. The cohesive beam bond is defined by two geometrical parameters (the length  $L_\mu$  and the radius  $R_\mu$ ) and two mechanical parameters (the Young's modulus  $E_\mu$  and the Poisson's ratio  $\nu_\mu$ ). These parameters are called microscopic parameters denoted by the symbol  $\mu$ . They are determined by a calibration process [2].

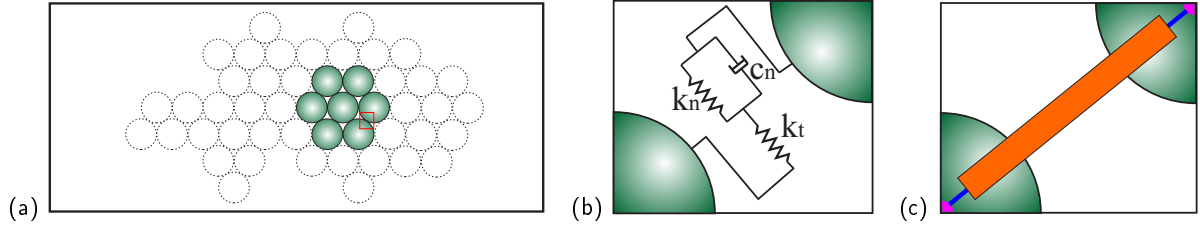


**Figure 2:** (a) DEM discretization of a continuous medium material, (b) the spring model and (c) cohesive beam model connect DEs.

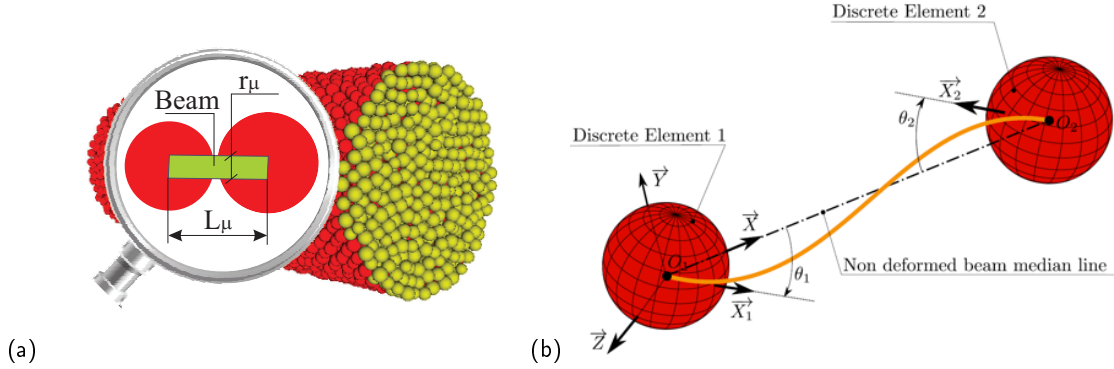


**Figure 3:** Illustration of the cohesive beam bond in GranOO at (a) relaxing state and (b) loading state [1]

**Table 1**  
Verlet dynamics explicit scheme

---

**Input:**  $\vec{p}(0), \vec{\dot{p}}(0), \vec{q}(0), \vec{\dot{q}}(0)$   
 $t \leftarrow 0$   
**for all** iteration  $n$  **do**  
  **for all** discrete element  $i$  **do**  
     $\vec{p}_i(t+dt) \leftarrow$  Linear position Verlet scheme (Eq.1)  
     $\vec{f}_i(t+dt) \leftarrow$  Sum of force acting on  $i$   
     $\vec{\ddot{p}}_i(t+dt) \leftarrow$  Acceleration from Newton's second law  
     $\vec{\dot{p}}_i(t+dt) \leftarrow$  Linear velocity Verlet scheme (Eq.2)  
  
     $\vec{q}_i(t+dt) \leftarrow$  Angular position Verlet scheme (Eq.3)  
     $\vec{M}_i(t+dt) \leftarrow$  Sum of momentum acting on  $i$   
     $\vec{\ddot{q}}_i(t+dt) \leftarrow$  Angular acceleration from momentum law  
     $\vec{\dot{q}}_i(t+dt) \leftarrow$  Angular velocity Verlet scheme (Eq.4)  
  **end for**  
   $t \leftarrow (t+dt)$   
**end for**

---

**Table 2**  
Mechanical properties of hemp yarn and epoxy matrix

Young's modulus of hemp yarn	10 GPa
Ultimate strain of hemp yarn	0.021
The radius of hemp yarn	150 $\mu\text{m}$
Matrix Young's modulus (epoxy)	3.322 GPa
Matrix Poisson's ratio	0.39
Matrix yield stress	69 MPa

### 3. Building the discrete domain

#### 3.1. Experimental basement

This study is based on the experimental results of a single fragmentation test [19]. Hemp yarn and epoxy matrix are considered. The mechanical properties of these materials are summarized in Tab.2.

The test configuration is shown in Fig.4. Type I and type II geometries have been retrained for specimens in order to ensure a sufficient stress triaxiality and properly initiate the

fragmentation process of the hemp yarn. Single yarn composite specimens were tested in uniaxial tensile loading with a load cell of 1 KN and a crosshead speed of 0.5 mm/min. In these tests, the stress field is revealed by the photoelasticity technique. Therefore, the specimens were placed into a circular polariscope during tensile loading (Fig.4b). Fig.5 shows the fragmentation stress  $\sigma_{frag}$  and longitudinal strain  $\epsilon_{frag}$  corresponding to each yarn fracture for both specimen geometries. The fragmentation process begins at the same strain  $\epsilon_{frag}$  (around 2.1%) for the different tested specimens. This value corresponds precisely to the single hemp yarn ultimate strain mentioned in (Tab.2) while the fragmentation stresses are completely different from the ultimate stress of the single yarn.

#### 3.2. The discrete domain creation

In this work, the middle part of a type I specimen is selected and modeled with DEM (Fig.6a). The discrete domain and its dimensions are shown in Fig.6b. A bi-disperse medium is elaborated for the composite. The DEs for model-

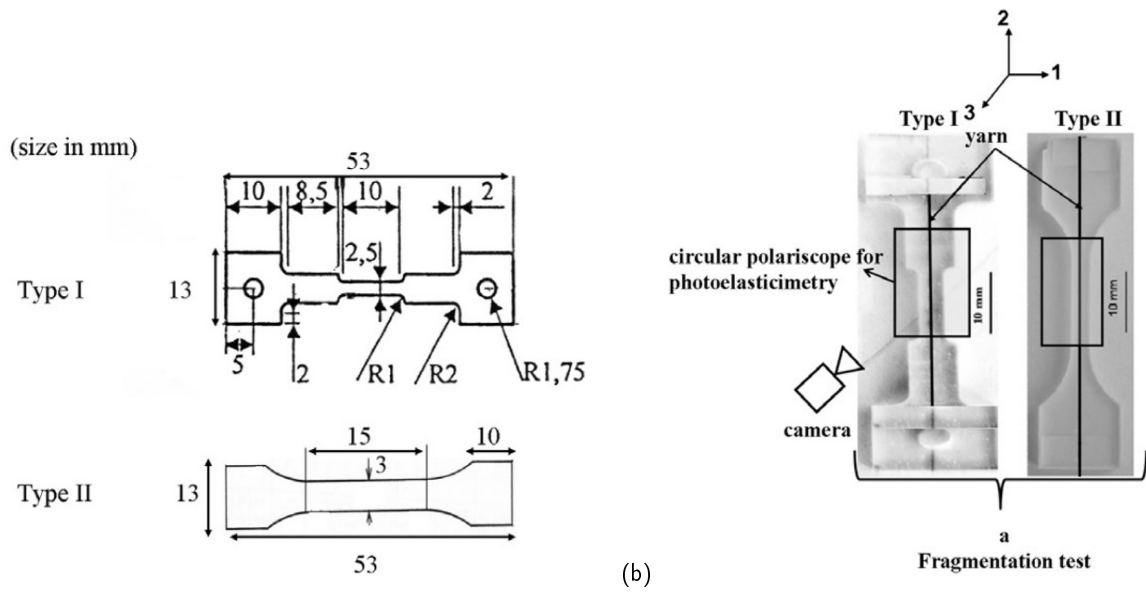


**Figure 4:** (a) Specimen geometry and (b) experimental technical used of 0° oriented single hemp yarn/epoxy composite specimen [19]

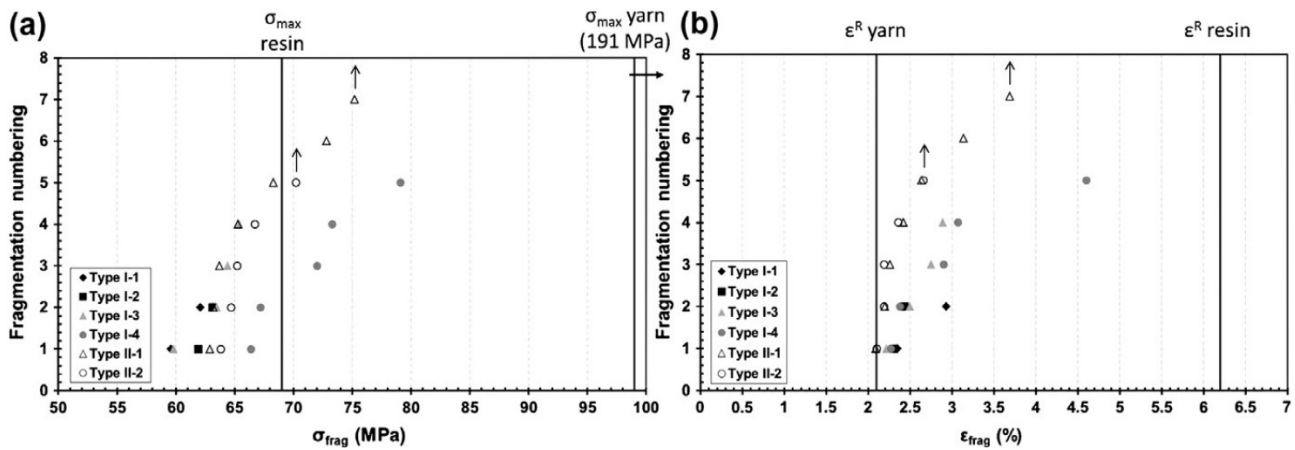


**Figure 5:** Stress (a) and strain (b) reached for each yarn fragmentation during fragmentation tests on single hemp yarn/epoxy composite specimens [19].

ing hemp yarn are greater than the ones for matrix. Indeed, for hemp yarn, the DE radius is equal to the radius of the yarn that supposed to be of circular cylindrical shape. The DEs are then stacked along the yarn with geometric continuity overlapping to properly represent the yarn/matrix interface. The overlap value between discrete element  $i$  and  $j$  of yarn is characterized by the ratio:  $d/(R_i + R_j)$ , with  $d = (R_i + R_j - O_i O_j)$  is the overlap value between discrete element  $i$  and  $j$ ,  $R_i = R_j$  are the radius of discrete element  $i$  and  $j$ , respectively.  $O_i O_j$  is the distance between centers of discrete elements  $i$  and  $j$  (Fig.7).

The discrete domain was created by a filling procedure. This procedure consists in building a compacted discrete domain [2] following the objectives: i) reach a rate of compaction for modeling correctly the continuum, ii) insure the medium isotropy (yarn and matrix are supposed to be isotropic),

iii) preserve the interface geometry ( yarn/matrix) as realistic as possible. The common filling procedure is performed in three distinct steps: i) a random free filling, ii) a forced filling, iii) a relaxation phase of the domain to prevent from residual stress state [2]. For the present bi-disperse medium, the construction of the discrete domain requires a special pre-filling step before engaging the filling procedure. In pre-filling step, the yarn DEs (Fig.8a) and a part of matrix DEs (Fig.8b) are placed in the middle of the domain. This matrix DEs part are regularly distributed in contact with yarn DEs. It allows a better description of the cohesion between yarn/matrix. These yarn and matrix DEs don't move during the filling process. Then, the three steps of filling procedure presented above are realized to build matrix. In the random free filling step, the matrix DEs (with a radius dispersion about 25%) are randomly placed in to the volume. This step

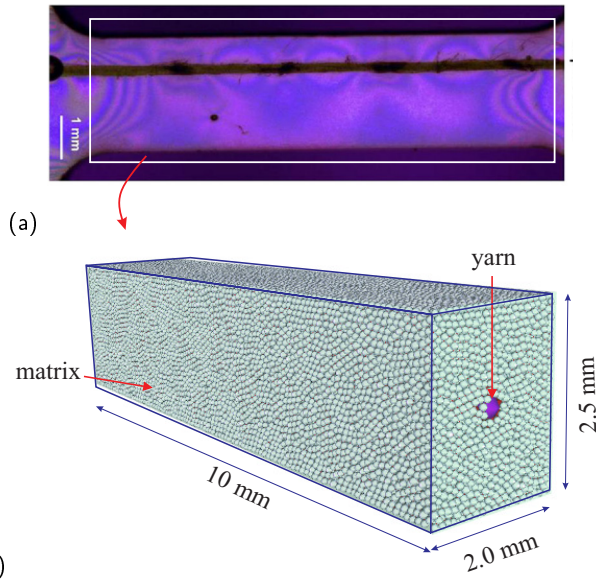


**Figure 6:** Middle part of Type I specimen: (a) experiment and (b) DEM.

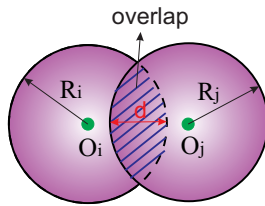


**Figure 7:** The overlap between two discrete elements of fiber.

ends when there is no more space to add a new DE without inter-penetration with each other (Fig.8c). The relaxation step allows to reduce the inter-penetrations between DEs and undesirable prestressed effects. It stops when the maximum inter-penetration value smaller than  $10^{-5}\%$  is reached. The compact discrete domain obtained after the filling procedure is shown in (Fig.8d).

#### 4. Mechanical modeling: cohesive beams, springs, cohesive contact at interface and matrix failure criteria

Once the geometry of the Type I specimen is achieved, the mechanical behavior is considered. For the bi-disperse medium, spring bonds are introduced to connect the DEs of the yarn while cohesive beams are used between the DEs of the matrix (Fig.9). Spring stiffness can be obtained analytically from the yarn mechanical properties. Only tension behavior is considered for yarn. All cohesive beams bond of DEM specimen are shown in Fig.10.

The DEM configuration of longitudinal and transversal section at yarn/matrix interface is presented in Fig.11. Cohesive contact laws taking place between the DE in contact at yarn/matrix interface are implemented. Piecewise linear laws are retained for modeling shear contact. This con-

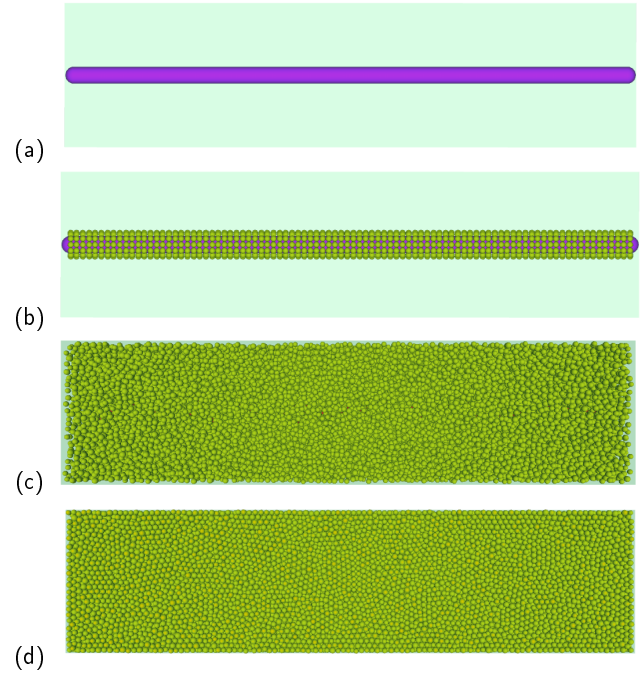


**Figure 8:** The pre-filling and filling procedure in DEM

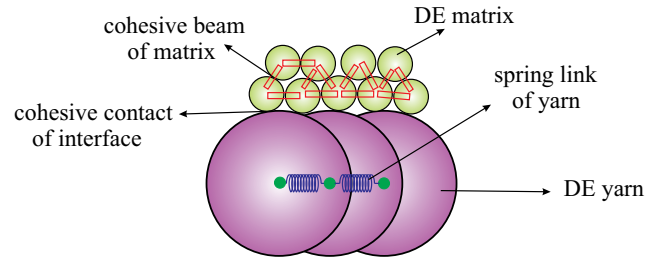


**Figure 9:** The configuration of mechanical bond and contact used in DEM.

tact softening model is quite similar to the Cohesive Contact Model (CCM) used in the continuum mechanics [42, 54]. The shear cohesive force is expressed as a function of the relative tangential displacement  $u_s$  between DEs of yarn and matrix in contact (Fig.12).  $u_s$  is calculated at each time step  $dt$ :  $u_s = \sum_{i=1}^N V_i dt$ , with  $N$  is the iteration number and  $V_i$  is the relative tangential velocity between two particles. The degradation of the interface begins when the displacements  $u_s$  reach the values  $u_s^e$  corresponding to the critical forces  $F_s^c$ . It continues until the displacements reach the values  $u_s^p$ . Detail of cohesive contact laws in DEM is presented in [28].

#### 4.1. Calibration of microscopic parameters

##### 4.1.1. Microscopic parameters of matrix epoxy and interface

In this study, the matrix DEs are connected by the cohesive beams whereas the fiber DEs are connected by the spring links (Fig.9). The cohesive beam has a cylindrical shape (Fig.3a) defined by two geometrical parameters (the length  $L_\mu$  and the radius  $r_\mu$ ) and two mechanical parameters (the Young's modulus  $E_\mu$  and the Poisson's ratio  $\nu_\mu$ )(see

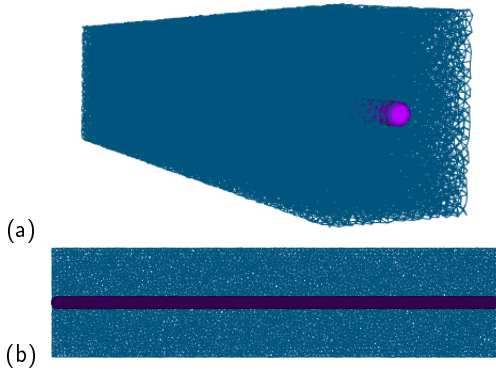


**Figure 10:** The cohesive beam bond of DEM specimen in (a) 3D and (b) longitudinal section.

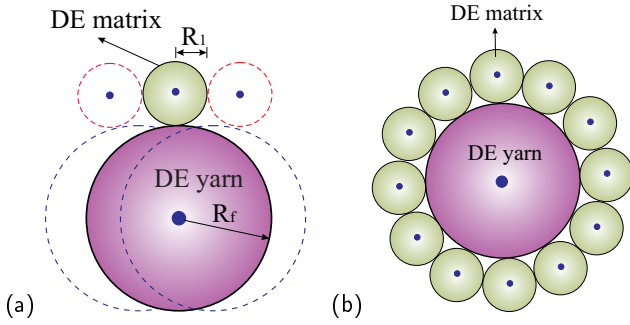


**Figure 11:** The configuration of (a) longitudinal and (b) transversal section in DEM at yarn/matrix interface.

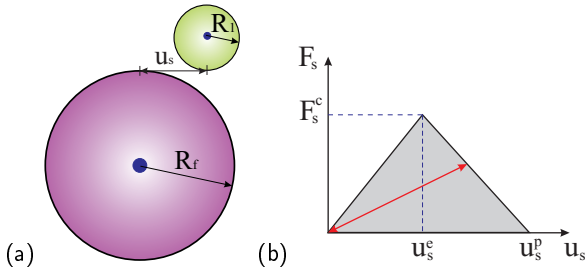


**Figure 12:** Constitutive of (a) shear displacement and (b) behavior of shear contact softening model between yarn/matrix.

Sec.2). By convenience, a radius ratio  $\tilde{r}_\mu$  is defined by  $\tilde{r}_\mu = r_\mu / \bar{R}_{DE}$  with ( $\bar{R}_{DE}$  being the average of discrete element radius). This value does not depend on the DE radius. The fracture behavior of this beam is driven by microscopic failure tensile stress  $\sigma_\mu$ . Above and hereafter, the subscript  $\mu$  always denotes the microscopic scale.

The cohesive beam length  $L_\mu$  is the distance between the centers of DEs interacting. The others microscopic parameters  $E_\mu$ ,  $\nu_\mu$ ,  $\tilde{r}_\mu$ ,  $\sigma_\mu$  are identified by the calibration process. This process is realized on a numerical tensile test with a cylinder specimen [2]. The discrete elements number used in this test is 10000.

André et al. [2] have observed that :

i) the microscopic Poisson's ratio  $\nu_\mu$  does not influence on the macroscopic Young's modulus  $E_M$  and the macroscopic

**Table 3**

Calibration of microscopic parameters of epoxy matrix

Matrix epoxy	$E_-$	$\nu_-$	$\sigma_-$	$\tilde{r}_-$	$\sigma_-$
Continuum properties $M$	3.322	0.39	69	-	-
Discrete properties $\mu$	580	0.39	-	0.16	246

The subscript  $-$  denotes  $M$  or  $\mu$ .

Poisson's ratio  $\nu_M$

ii) the macroscopic Poisson's ratio  $\nu_M$  depends only on the microscopic radius ratio  $\tilde{r}_\mu$

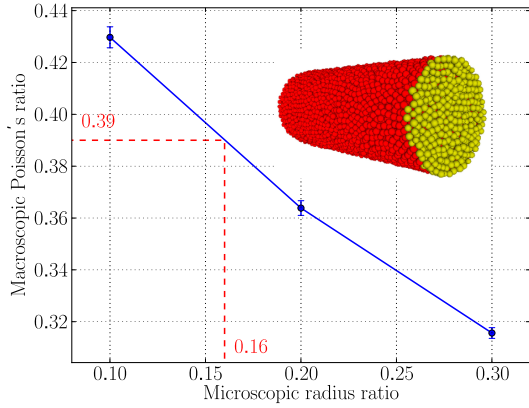
iii) the macroscopic Young's modulus  $E_M$  depends on the microscopic radius ratio  $\tilde{r}_\mu$  and the microscopic Young's modulus  $E_\mu$ .

Based on these observations, the microscopic parameters of cohesive beam can be determined by the calibration process following below steps :

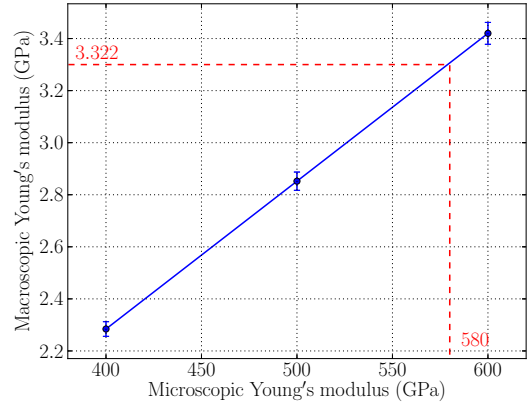
- choose arbitrary initial values for  $\nu_\mu$  and  $E_\mu$  ( $\nu_\mu = 0.39$  and  $E_\mu = 1000 \text{ GPa}$ ). Then,  $\tilde{r}_\mu$  is varied with each numerical tensile test. Three value of  $\tilde{r}_\mu$ : 0.1, 0.2, 0.3 are used. The numerical results allows to establish the calibration curve of  $\nu_M$  versus  $\tilde{r}_\mu$  (Fig.13a). The value of  $\tilde{r}_\mu$  is identified from this calibration curve, which corresponds to the macroscopic value  $\nu_M$ . With the macroscopic Poisson's ratio value of present material  $\nu_M = 0.39$ , the microscopic radius ratio  $\tilde{r}_\mu = 0.16$  is found.
- knowing the value of  $\tilde{r}_\mu = 0.16$ , the microscopic Young's modulus  $E_\mu$  varies for three tensile tests:  $E_\mu = 400 \text{ GPa}$ ,  $E_\mu = 500 \text{ GPa}$ ,  $E_\mu = 600 \text{ GPa}$ . The calibration curve of macroscopic Young's modulus  $E_M$  versus the microscopic Young's modulus  $E_\mu$  is obtained in Fig.13b. The microscopic Young's modulus  $E_\mu = 580 \text{ GPa}$  corresponds to the desired macroscopic Young's modulus  $E_M = 3.322 \text{ GPa}$  can be obtained.
- knowing the elastic parameters at microscopic scale ( $\tilde{r}_\mu = 0.16$ ,  $E_\mu = 580 \text{ GPa}$ ,  $\nu_\mu = 0.39$ ), the tensile test on the same specimen is realized to determine the microscopic failure stress  $\sigma_\mu$ . Three values of  $\sigma_\mu$ : 100 GPa, 200 GPa, 300 GPa are used. The failure criteria is Removed DE Failure process (RDEF), detailed in Sec.4.2. The calibration curve of macroscopic failure stress  $\sigma_M$  versus the microscopic failure stress  $\sigma_\mu$  is established on Fig.14. For  $\sigma_M = 69 \text{ GPa}$ , the value of  $\sigma_\mu = 246 \text{ GPa}$  is obtained.

All the microscopic parameters of the discrete domain after calibration process ( $\tilde{r}_\mu$ ,  $E_\mu$ ,  $\nu_\mu$ ,  $\sigma_\mu$ ) are listed in Tab.3.

For the interface yarn/epoxy, CCM is introduced (Fig.12). The microscopic parameters of the cohesive contact model are ( $u_s^e$ ,  $u_s^p$ ,  $F_s^c$ ).  $F_s^c$  is the maximum of shear cohesive force at interface between DEs of yarn and epoxy. This force links with the interfacial shear strength by  $F_s^c = \sigma_s^c S_m$ , with  $\sigma_s^c$  is



(a)



(b)

**Figure 13:** Calibration curves: (a) Radius ratio  $\tilde{r}_\mu$  calibration and (b) microscopic Young's modulus  $E_\mu$  calibration.

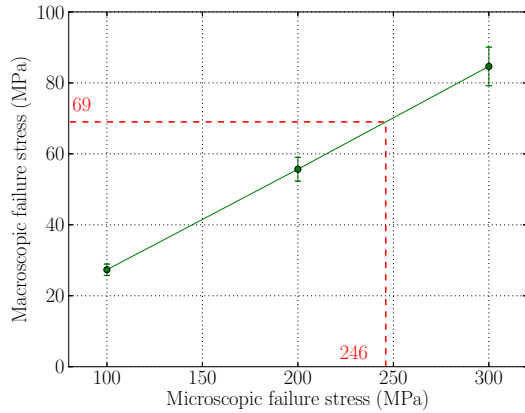


**Figure 14:** Calibration curves: microscopic failure stress  $\sigma_\mu$  calibration.

the interfacial shear strength,  $S_m = \pi R_1^2$  is the area of contact surface, with  $R_1$  is the radius of matrix DE in contact with the yarn. These values are inspired from literature [19],  $\sigma_s^c = 21 \text{ MPa}$ ,  $u_s^p = 0.02 \text{ mm}$ ,  $u_s^e = 0.01 \text{ mm}$ .

#### 4.1.2. Microscopic parameters of hemp yarn

Fig.15 presents the configuration of hemp yarn in continuous and discrete medium. In DEM, the DEs of yarn are superimposed and connected by the spring links (the DEs overlapping is 90%) (Fig.15b,c). The stiffness  $k_n$  of spring  $n$  arranged in series can be easily related to the stiffness  $K$  of the yarn, Eq.(5):

$$\frac{1}{K} = \sum_{n=1}^N \frac{1}{k_n} \quad K = \frac{ES}{L} \quad (5)$$

where  $N$  is the number of springs,  $E$  is the yarn Young's modulus,  $S = \pi R_f^2$  is the cross-section of the yarn with its radius  $R_f$  and  $L$  denotes the yarn length (Fig.15).

The numerical result of tensile test on singer yarn is shown

on Fig.16. A good convergence between numerical and theoretical results of Young's modulus is obtained (Fig.16a). The maximum strain criterion is used for the rupture of yarn. A very good agreement for the failure strain is identified between numerical and experiment (Fig.16b).

#### 4.2. Failure criterion for the matrix

The matrix is modeled as an homogeneous and isotropic brittle material. The failure criteria used is Removed DE Failure process (RDEF) [3, 21]. It leads to the deletion of a DE when a tensile criterion is satisfied in bonds connected to this DE Fig.17.

The virial tensor is defined for each DE as follows:

$$\bar{\sigma}_i = \frac{1}{2\Omega_i} \sum_{j \neq i} \frac{1}{2} (\vec{r}_{ij} \otimes \vec{f}_{ij} + \vec{f}_{ij} \otimes \vec{r}_{ij}) \quad (6)$$

where :

- $\otimes$  is the tensor product
- $\bar{\sigma}_i$  is the equivalent Cauchy stress tensor for the discrete element  $i$
- $\Omega_i$  is an influential volume around the discrete element  $i$
- $\vec{f}_{ij}$  is the force exerted on the discrete element  $i$  by a cohesive beam that bonds the discrete element  $i$  to another discrete element  $j$
- $\vec{r}_{ij}$  is the relative position vector between the center of the two bonded discrete elements  $i$  and  $j$

The criterion assumes that fracture occurs when the hydrostatic stress is higher than a threshold critical value  $\sigma_c$  [3]:

$$\frac{1}{3} \text{trace} (\bar{\sigma}_i) \geq \sigma_{fail} \quad (7)$$

When the criterion is satisfied, all the cohesive beams in  $\Omega_i$  around the discrete element  $i$  are broken ( Fig.17).

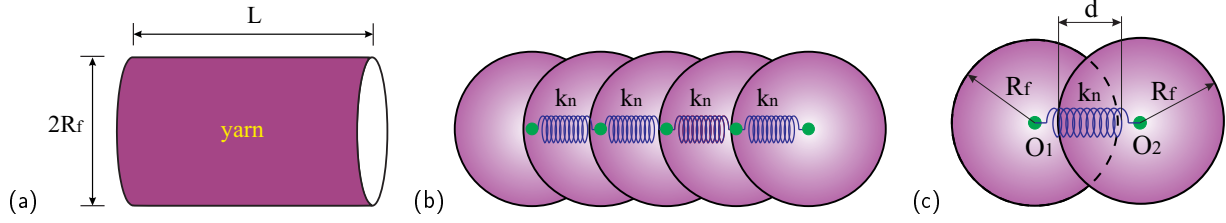


**Figure 15:** Yarn modeling : (a) continuous medium, (b,c) the spring link connected the DEs of yarn in DEM

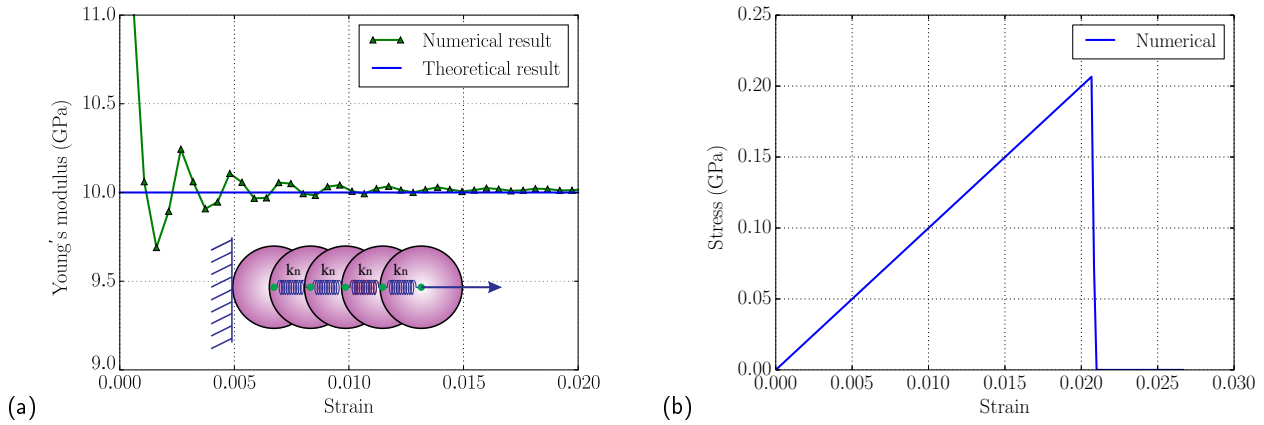


**Figure 16:** The numerical results of singer yarn test in (a) elastic and (b) fracture.

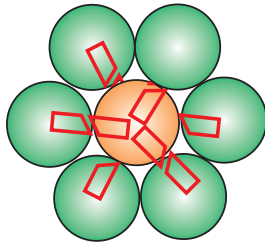


**Figure 17:** Illustration of breaking bond for RDEF criterion

The microscopic failure tensile stress  $\sigma_{fail} = 246 \text{ MPa}$  is also determined by the calibration procedure which is detailed in Sec.4.1.1.

## 5. Numerical results

Knowing all the microscopic parameters of discrete domain ( $r_\mu$ ,  $E_\mu$ ,  $\nu_\mu$ ,  $\sigma_\mu$ ) (see Tab.3), a fragmentation test was performed. This test is based on experimental test reminded in Sec.3.1 and presented in [19]. A uniform displacement  $u$  is imposed at the right and left edges of specimen (Fig.18). The numerical specimen contains 66619 DEs of matrix (with the mean radius of  $5.10^{-2} \text{ mm}$ ) and 324 DEs of yarn.

The comparison of Young's modulus of composite specimen during the fragmentation test is presented in Fig.19. A good agreement results is obtained between experiment, analytic, finite element model (FEM) and DEM. The analytical value of Young's modulus is identified based on Eq.(8). With,  $E_m$ ,  $V_m$ ,  $E_f$ ,  $V_f$  are Young's modulus and volume

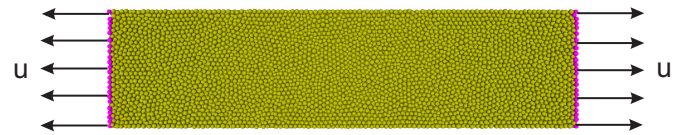


**Figure 18:** Uniform displacement impose at two opposite face of numerical specimen.

fraction of matrix and yarn, respectively.

$$E = E_m V_m + E_f V_f \quad (8)$$

The result of numerical and experimental stress-strain curve is presented in Fig.20. A good tendency in elastic part is obtained between FEM, DEM and experiment. However, a significant difference in trend is observed when the strain evolution and greater than 0.014. A more brittle behavior is obtained with DEM. This result is explained by the different matrix failure criterion used in each simulation methods FEM and DEM. In DEM, the matrix follows a linear fracture model whereas a elasto-plastic behavior law is used in FEM.

Fragmentation process starts when the strain criterion is satisfied in the hemp yarn. Fig.21 shows the final fragmentation result during the test. A similar number of fragmentation (4 fragmentations) is obtained between experimental, FEM and DEM modeling. In addition, these fragmentations are almost located at the same position.

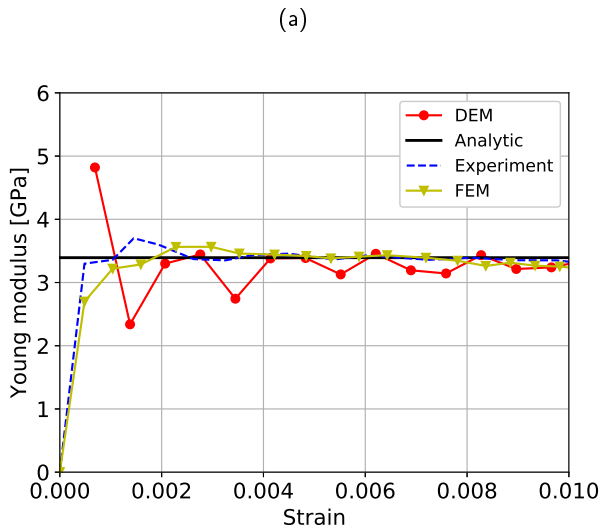


**Figure 19:** Result of Young's modulus during the fragmentation test.

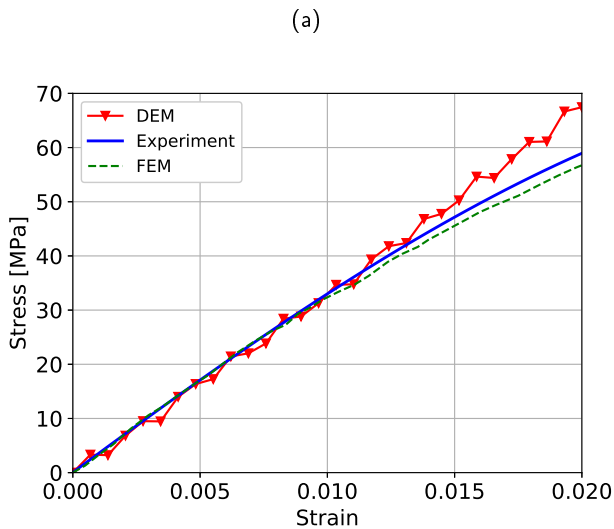


**Figure 20:** Numerical and experimental stress-strain curves

## 6. Conclusion

A 3D simulation of interface debonding in composite material using DEM is investigated in this study. It is based on the experimental results of a single fragmentation testing obtained by Guillebaud-Bonafous and al. [19]. The composite material uses an impregnated hemp yarn embedded into a epoxy matrix. In DEM, matrix and yarn are supposed to be brittle materials and follow a linear fracture model. The DEs of matrix are connected by the cohesive beams bond whereas the DEs of yarn are connected by the spring links. The mechanical properties of these bonds are identified by a calibration procedure. The cohesive zone models is implemented to model interface debonding between yarn and matrix. The bi-disperse medium in DEM for matrix and yarn is specifically elaborated in this study to reduce the discrete elements number and save computational time. The numerical results obtained by DEM are compared with experimen-

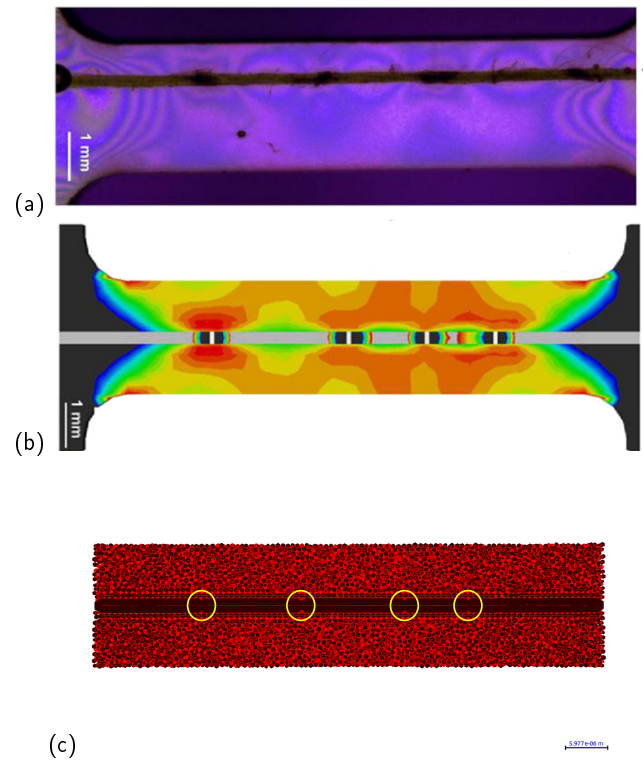


**Figure 21:** Comparison of (a) experimental, (b) FEM and (c) DEM for the fragmentation during the test.

tal and FEM results on the stress-strain curve and the fragmentation process in yarn during the test. A good agreement results of Young's modulus is obtained between experiment, analytic, FEM and DEM. It corresponds to a good tendency in elastic part of the stress-strain curve in: experiment, FEM and DEM. A more brittle behavior is obtained with DEM. This result is explained by the different matrix failure criterion used in each simulation methods FEM and DEM. Concerning the fragmentation process, a similar number and position of fragmentation is obtained between experimental, FEM and DEM modeling. These promising results allow to validate the models used in DEM (cohesive beams bond to model the mechanical behavior of matrix, spring links to model the mechanical behavior of yarn and cohesive zone models to model the mechanical behavior of interface yarn/matrix).

## References

- [1] André, D., Charles, J.I., Iordanoff, I., Néauport, J., 2014. The GranOO workbench, a new tool for developing discrete element simulations, and its application to tribological problems. *Engineering Software* 74, 40–48.
- [2] André, D., Iordanoff, I., Charles, J.I., Néauport, J., 2012. Discrete element method to simulate continuous material by using the cohesive beam model. *Comput Methods Appl Mech Engng* vol.231-216, 113–125.
- [3] André, D., Jebahi, M., Iordanoff, I., Charles, J.I., Néauport, J., 2013. Using the discrete element method to simulate brittle fracture in the indentation of a silica glass with a blunt indenter. *Comput Methods Appl Mech Engng* 265, 136–147.
- [4] Awal, A., Cescutti, G., Ghosh, S., Müssig, J., 2011. Interfacial studies

- of natural fibre/polypropylene composites using single fibre fragmentation test (sfft). *Composites Part A: Applied Science and Manufacturing* 42, 50–56.
- [5] Aymerich, F., Dore, F., Priolo, P., 2008. Prediction of impact-induced delamination in cross-ply composite laminates using cohesive interface elements. *Composites Science and Technology* 68(12), 2383–2390.
  - [6] Babaei, R., Farrokhabadi, A., 2020. Prediction of debonding growth in two-dimensional rves using an extended interface element based on continuum damage mechanics concept. *Composite Structures* 238, 111981.
  - [7] Bechel, V., Sottos, N., 1998. Application of debond length measurements to examine the mechanics of fiber pushout. *J. Mech. Phys. Solids* 46, 1675–1697.
  - [8] Bogoeva-Gaceva, G., Miider, E., Hiublner, L., Sahre, K., 1995. Parameters affecting the interface properties in carbon fibre/epoxy systems. *Composites* 26, 103–107.
  - [9] Camanho, P.P., Davila, C.G., De Moura, M.F., 2003. Numerical simulation of mixed-mode progressive delamination in composite materials. *Journal of Composite Master* 37, 1415–1438.
  - [10] Carmona, H.A., Wittel, F.K., Kun, F., Herrmann, H.J., 2008. Fragmentation processes in impact of spheres. *Physical Review* 77(5), 051302.
  - [11] Cheng, T.H., Jones, F., Wang, D., 1993. Effect of fibre conditioning on the interfacial shear strength of glass-fibre composites. *Composites Science and Technology* 48, 89–96.
  - [12] Crisfield, M.A., Alfano, G., 2000. Finite element interface models for the delamination analysis of laminated composites: mechanical and computational issues. *Int J Num Meth Eng* 50, 1701–1736.
  - [13] Cundall, P.A., Strack, O.D.L., 1979. A discrete numerical model for granular assemblies 29, 47–65.
  - [14] Delaplace, A., Desmorat, R., 2007. Discrete 3d model as complementary numerical testing for anisotropic damage. *International Journal of Fracture* 148, 115–128.
  - [15] Drzal, L.T., Rich, M.J., Lloyd, P.F., 1983. Adhesion of graphite fibers to epoxy matrices: I. the role of fiber surface treatment. *The Journal of Adhesion* 16, 1–30.
  - [16] Eberly, D., 2010. Game physics.
  - [17] Goh, K., Aspden, R.M., Hukins, D.W.L., 2004. finite element analysis of stress transfer in short-fibre composite materials. *Composites science and technology* 64, 1091–1100.
  - [18] Goh, K., Mathias, K., Aspden, R., Hukins, D., 2000. Finite element analysis of the effect of fibre shape on stresses in an elastic fibre surrounded by a plastic matrix. *Journal of materials science* 35, 2493–2497.
  - [19] Guillebaud-Bonafous, C., Vasconcellos, D., Touchard, F., Chocinski-Arnault, L., 2012. Experimental and numerical investigation of the interface between epoxy matrix and hemp yarn. *Composites: Part A* 43, 2046–2058.
  - [20] Hu, N., Zemba, Y., Okabe, T., Yan, C., Fukunaga, H., Elmarakbi, A.M., 2008. A new cohesive model for simulating delamination propagation in composite laminates under transverse loads. *Mechanics of Materials* 40(11), 920–935.
  - [21] Jebahi, M., André, D., Dau, F., Charles, J.L., Iordanoff, I., 2013. Simulation of Vickers indentation of silica glass. *J Non Cryst Sol* 378, 15–24.
  - [22] Johnson, A., Zhao, F., Hayes, S., Jones, F., 2006. Influence of a matrix crack on stress transfer to an  $\alpha$ -alumina fibre in epoxy resin using fea and photoelasticity. *Composites science and technology* 66, 2023–2029.
  - [23] Kelly, A., Tyson, a.W., 1965. Tensile properties of fibre-reinforced metals: copper/tungsten and copper/molybdenum. *Journal of the Mechanics and Physics of Solids* 13, 329–350.
  - [24] Kim, B.W., Nairn, J.A., 2002. Observations of fiber fracture and interfacial debonding phenomena using the fragmentation test in single fiber composites. *Journal of Composite Materials* 36, 1825–1858.
  - [25] Kim, J., Mai, Y., 1991. High strength, high fracture toughness fibre composites with interface control-a review. *Composites Science and Technology* 41(4), 333–378.
  - [26] Koval, G., Le, B.D., Chazallon, C., 2016. Discrete element model for quasi-brittle rupture under tensile and compressive loading. *International Journal for Numerical and Analytical Methods in Geomechanics* 40, 2339–2352.
  - [27] Kun, F., Herrmann, H.J., 1996. A study of fragmentation processes using a discrete element method. *Computer Methods in Applied Mechanics and Engineering* 138(1-4), 3–18.
  - [28] Le, B.D., Dau, F., Charles, J.L., Iordanoff, I., 2016a. Modeling damages and cracks growth in composite with a 3d discrete element method. *Composites Part B: Engineering* 91, 615–630.
  - [29] Le, B.D., Koval, G., Chazallon, C., 2013. Discrete element approach in brittle fracture mechanics. *Engineering Computations* 30(2), 263–276.
  - [30] Le, B.D., Koval, G., Chazallon, C., 2016b. Discrete element model for crack propagation in brittle materials. *International Journal for Numerical and Analytical Methods in Geomechanics* 40, 583–595.
  - [31] Liu, H.Y., Mai, Y.W., Zhou, L.M., Ye, L., 1994. Simulation of the fibre fragmentation process by a fracture mechanics analysis. *Composites science and technology* 52, 253–260.
  - [32] Maheo, L., Dau, F., André, D., Charles, J.L., Iordanoff, I., 2015. A promising way to model cracks in composites using a Discrete Element Method. *Composites part B* 71, 193–202.
  - [33] Matsuda, Y., Iwase, Y., 2002. Numerical simulation of rock fracture using three-dimensional extended discrete element method. *Earth Planets Space* 54, 367–378.
  - [34] Meo, M., Thieulot, E., 2008. Delamination modelling in a double cantilever beam. *Composite Structures* 71(3-4), 429–434.
  - [35] Miller, B., Muri, P., Rebenfeld, L., 1987a. A microbond method for determination of the shear strength of a fiber/resin interface. *Composites Science and Technology* 28, 17–32.
  - [36] Miller, B., Muri, P., Rebenfeld, L., 1987b. A microbond method for determination of the shear strength of a fiber/resin interface. *Composites Science and Technology* 28, 17–32.
  - [37] Mohammad, J.K., Ahmed, K., 2013. Modeling tensile response of fiber-reinforced polymer composites using discrete element method. *Polymer Composites* 34, 877–886.
  - [38] Naghdinasab, M., Farrokhabadi, A., Madadi, H., 2018. A numerical method to evaluate the material properties degradation in composite rves due to fiber-matrix debonding and induced matrix cracking. *Finite Elements in Analysis and Design* 146, 84–95.
  - [39] Nath, R., Fenner, D., Galiotis, C., 2000. The progressional approach to interfacial failure in carbon reinforced composites: elasto-plastic finite element modelling of interface cracks. *Composites Part A: Applied Science and Manufacturing* 31, 929–943.
  - [40] Nishikawa, M., Okabe, T., Hemmi, K., N., T., 2008a. Micromechanical modeling of the microbond test to quantify the interfacial properties of fiber-reinforced composites. *International Journal of Solids and Structures* 45, 4098–4113.
  - [41] Nishikawa, M., Okabe, T., Hemmi, K., Takeda, N., 2008b. Micromechanical modeling of the microbond test to quantify the interfacial properties of fiber-reinforced composites. *International Journal of Solids and Structures* 45, 4098–4113.
  - [42] Nishikawa, M., Okabe, T., Takeda, N., 2007. Numerical simulation of interlaminar damage propagation in CFRP cross-ply laminates under transverse loading. *Engineering Fracture Mechanics* 44(10), 3101–3113.
  - [43] Nishikawa, M., Okabe, T., Takeda, N., Curtin, W., 2008c. Micromechanics of the fragmentation process in single-fiber composites. *Modelling and Simulation in Materials Science and Engineering* 16, 055009.
  - [44] Okabe, T., Takeda, N., 2002. Elastoplastic shear-lag analysis of single-fiber composites and strength prediction of unidirectional multi-fiber composites. *Composites Part A: Applied Science and Manufacturing* 33, 1327–1335.
  - [45] Pinho, S.T., Ianucci, L., Robinson, P., 2006. Formulation and implementation of decohesion elements in an explicit finite element code. *Compos A: Appl Sci Manufactur* 37, 778–789.

- [46] Potyondi, D.O., Cundall, P.A., 2004. A Bonded-Particle Model for Rock. *Int. J. Rock Mech. Min. Sci.* 41, 1329–1364.
- [47] Sheng, Y., Yang, D., Ye, J., Tan, Y., 2010. Modeling progressive delamination of laminated composites by discrete element method. *Composites Science and Technology* 70, 2093–2101.
- [48] Takada, S., Hassani, N., 1996. *Earthquake Resistant Engineering Structures*. Computational Mechanics Publications. volume 23. chapter Analysis of compression failure of reinforced concrete by the modified distinct element method.
- [49] Tavarez, F.A., Plesha, M.E., 2007. Discrete element method for modelling solid and particulate materials. *International journal for numerical methods in engineering* 70, 379–404.
- [50] Tripathi, D., Chen, F., Jones, F.R., 1996. The effect of matrix plasticity on the stress fields in a single filament composite and the value of interfacial shear strength obtained from the fragmentation test. *Proceedings of the Royal Society of London. Series A: Mathematical, Physical and Engineering Sciences* 452, 621–653.
- [51] Tripathi, D., Jones, F., 1998. Single fibre fragmentation test for assessing adhesion in fibre reinforced composites. *Journal of materials science* 33, 1–16.
- [52] Wittel, F.K., Kun, F., Kroplin, B.H., Herrmann, H.J., 2003a. A study of transverse ply cracking using a discrete element method. *Comput Mater Sci* 28(3-4), 608–619.
- [53] Wittel, F.K., Schulte-Fischedick, J., Kun, F., Kropolin, B.H., Frieb, M., 2003b. Discrete element simulation of transverse cracking during the pyrolysis of carbon fibre reinforced plastics to carbon/carbon composites. *Comput Mater Sci* 28, 1–15.
- [54] Xie, D., Waas, A.M., 2006. Discrete cohesive zone model for mixed-mode fracture using finite element analysis. *Engineering Fracture Mechanics* 73(13), 1783–1796.
- [55] Yang, D., Sheng, Y., Ye, J., Tan, Y., 2010. Discrete element modeling of the microbond test of fiber reinforced composite. *Computational Materials Science* 49, 253–259.
- [56] Yang, D., Sheng, Y., Ye, J., Tan, Y., 2011. Modeling progressive delamination of laminated composites by discrete element method. *Computational Materials Science* 50, 858–864.
- [57] You, J., Lutz, W., Gerger, H., Siddiq, A., Brendel, A., HÄütschen, C., Schmauder, S., 2009. Fiber push-out study of a copper matrix composite with an engineered interface: Experiments and cohesive element simulation. *International Journal of Solids and Structures* 46, 4277–4286.